

# An experimental study on creep of welded tuff

L. Ma<sup>a,\*</sup>, J.J.K. Daemen<sup>b</sup>

<sup>a</sup>Vector Engineering, Inc., Grass Valley, CA 95945, USA

<sup>b</sup>Department of Mining Engineering, University of Nevada, Reno, NV 89557, USA

Accepted 28 July 2005

Available online 12 September 2005

## Abstract

This paper presents results of five creep tests conducted in uniaxial compression at room temperature. The test specimens were from the welded Topopah Spring tuff formation at Yucca Mountain, Nevada. The specimens exhibited brittle failure. Multiple stress levels were applied in steps to each specimen. Each stress level was maintained for 3 days or longer. The transient creep for all the stress levels can be well described by power functions. The transient creep is caused by an elastic aftereffect. The tuff does not show real steady-state creep. The so-called steady-state creep rate decreases with time. In general it is very low, typically in the range of  $10^{-7} \text{ h}^{-1}$ . For the first 50 h, the so-called steady-state creep rate may be described as a power function of stress. The specimen failed shortly after it entered into the accelerating creep phase.

© 2005 Elsevier Ltd. All rights reserved.

*Keywords:* Creep; Tuff; Uniaxial; Brittle; Steady-state creep

## 1. Introduction

### 1.1. Test description

Yucca Mountain has been selected as a candidate site for a high level nuclear waste repository in the United States [1]. The repository is to be excavated in the welded Topopah Spring tuff. Units exposed in the Topopah Spring tuff include the Topopah Spring crystal-poor upper lithophysal zone (Tptpul), the Topopah Spring crystal-poor middle nonlithophysal zone (Tptpmn), the Topopah Spring crystal-poor lower lithophysal zone (Tptpll), and the Topopah Spring crystal-poor lower nonlithophysal zone (Tptpln) [2]. Among the five tests, one specimen was from the lower nonlithophysal zone and the other four from the middle nonlithophysal zone. The purpose of the tests was to investigate the long-term mechanical behavior of the tuff.

The specimens were prepared from rock cores received from the sample management facility (SMF), Yucca Mountain Site Characterization Project. The nominal diameters of the cores were 61 and 45 mm. The specimens were cut to a ratio of length to diameter of 1.9–2.4, to approximately meet ASTM D 4543 [3]. The specimens were selected so that they did not contain major lithophysae or visible fissures (Fig. 1). Vapor-phase altered spots were common among the rock cores. Small vapor-phase altered inclusions were allowed in the specimens selected for the tests (Fig. 1a). Lithophysae are gas-formed voids created soon after emplacement of the ash-flow tuff. Vapor-phase altered spots are regions of tuff matrix altered by gases in the early stages of tuff emplacement [4].

Moisture contents for the specimens were measured soon after testing. The average value was 0.58%. The porosity of the welded Topopah Spring tuff is in the range of 10–13% [5–8]. Table 1 summarizes the specimen source information, dimensions and moisture contents.

The tests were conducted in a 2670 kN (600 kip) material testing system (MTS), stiff servo-controlled

\*Corresponding author. Tel.: +1 530 272 2448;  
fax: +1 530 272 8533.

E-mail address: [ma@vectoreng.com](mailto:ma@vectoreng.com) (L. Ma).

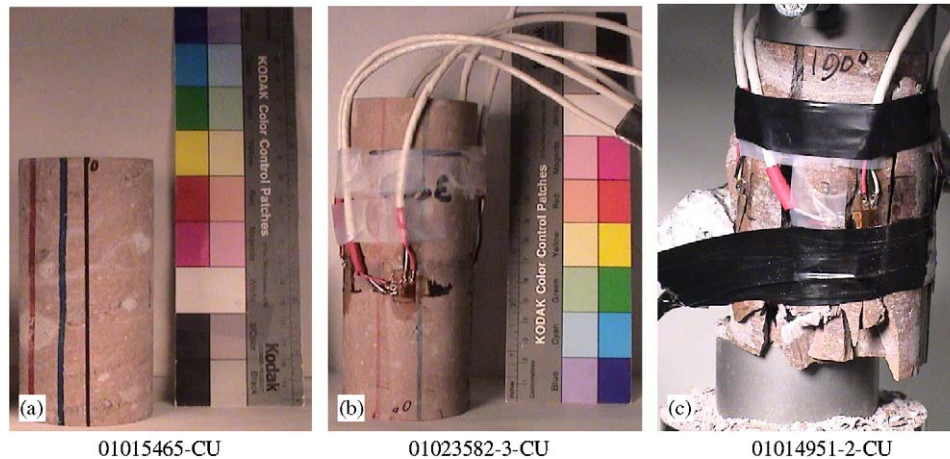


Fig. 1. Specimens for creep testing: (a) contains vapor-phase altered spots; (b) has strain gages installed; (c) shows failure pattern.

Table 1  
Specimen source information, dimensions and moisture contents

Specimen	Source		Diameter (mm)	Length (mm)	Moisture content
	Borehole	Zone			
01023363-1-CU	ESF-MD-NICHE 3107#7	Tptpmn	45	105.16	0.45%
01023364-1-CU	ESF-MD-NICHE 3107#7	Tptpmn	45	105.41	0.43%
01023665-2-CU	ESF-HD-WH-36	Tptpmn	61	124.21	0.71%
01023582-3-CU	ESF-HD-WH-5	Tptpmn	61	145.03	0.72%
01015465-CU	USW SD-12	Tptpln	61	116.08	N/A

hydraulic test frame. Load was measured using a load cell. Strain was measured using self-temperature-compensated electrical resistance strain gages. Six strain gages were used on each specimen. Four measured axial strain and two measured lateral strain. Strain gages were cemented at about midheight of each specimen (Fig. 1b). Strain in each direction was calculated by averaging all measurements in that direction.

Test temperature was monitored using thermocouples. Significant temperature variation was observed in some tests. The variation came from three sources: (1) alternation of days and nights, (2) heat generated in the MTS test system, (3) unexpected adjustment of room air conditioning. Of the three above, the first and the second accompanied all the tests. The range of variation for the two sources usually was about 3–5 °C. The third source occurred several times. The maximum temperature fluctuation caused by this source in a single stress level was as high as 8.6 °C (occurred in test 01023582-3-CU, stress level of 173.38 MPa). The temperature variation generated thermal output or temperature-induced strain. The temperature-induced strain was a part of strain measurement registered in the strain indicator, and it significantly altered the strain measurements. The Topopah Spring tuff exhibited a very low

creep rate, typically in the order of  $10^{-7} \text{ h}^{-1}$  during the steady-state phase. Given the low creep rate, even a small change in test temperature (say 3–5 °C) could make the measured creep rate difficult to interpret.

The temperature-induced strain was caused by two concurrent effects in the strain gage installation. First, the electrical resistivity of the grid conductor is temperature dependent, and, as a result, the gage resistance varies with temperature. The second contribution to thermal output is due to the differential thermal expansion between the grid conductor and the specimen. In this study the first is minor. For the second, using self-temperature-compensated strain gages could eliminate the thermal output if the thermal expansion coefficient in the strain gages would match the one in the specimen. However, it is difficult to select a type of strain gage to match perfectly the tuff specimens in thermal expansion coefficients. One obvious fact is that the thermal expansion coefficient from specimen to specimen would not be unique because of the complexity of the microstructure of the tuff. To remedy the temperature effect, a multivariate regression approach is adopted in this study to remove the thermal output from the strain measurement. The detailed procedure is described in the Appendix.

## 1.2. Mechanism of deformation in brittle rocks

All specimens exhibited brittle failure. The major fractures were nearly parallel to the axes of the specimens by predominantly longitudinal splitting (Fig. 1c). A considerable number of investigations on deformation in brittle rocks have been conducted within the past 40 years [9,10]. It has been widely accepted that the main mechanism of inelastic deformation in brittle rocks under uniaxial compression is the development of cracks parallel to the compressive stress direction [11–21]. Rock is a polycrystalline aggregate generally of several anisotropic phases. If a uniform stress is applied to such an inhomogeneous material, the local stress at a point will not, in general, be the same as the applied stress but will vary in some complex way throughout the body [22]. This inhomogeneity is the basic factor governing the microfracturing of rock [23,24].

## 2. Results, analysis and discussion

Creep is typically reported in terms of three distinct phases: transient creep, steady-state creep and accelerating creep. For rocks with a large variability in properties (e.g. strength) such as the Topopah Spring tuff, the ultimate strength of various specimens is highly variable. It is difficult to complete a creep test with a single stress level within months, because it is difficult to select a stress level that will assuredly give creep without instantaneously leading to failure. In this study multiple stress levels were applied in steps to each specimen. Each stress level was maintained for no less than 3 days. The stress increment from one level to the next was 7–10 MPa. The tests took from 2 to 13 stress steps. The longest test lasted 1206.3 h (50.3 days). Fig. 2 gives the complete axial strain–time curves for the five tests. Compressive normal stresses and longitudinal strains are positive. Table 2 summarizes the test durations, starting stresses and ultimate strengths for the tests.

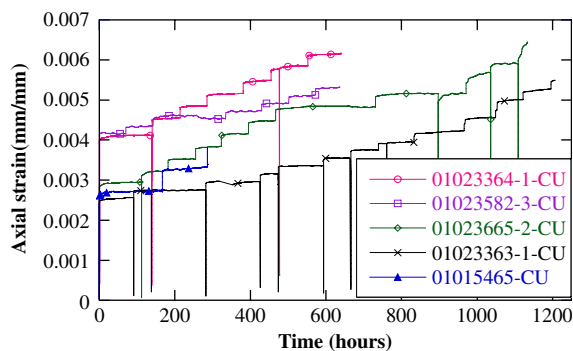


Fig. 2. Axial strain–time curves for the five tests.

Table 2

Test durations, starting stresses and ultimate strengths

Test	Test duration (h)	1st stress level (MPa)	Ultimate strength ( $\sigma_c$ , MPa)
01023363-1-CU	1206.3	93.79	168.77
01023364-1-CU	617.7	137.53	193.77
01023665-2-CU	1132.9	102.00	195.29
01023582-3-CU	637.0	159.67	200.79
01015465-CU	287.7	102.00	143.93

As soon as the axial stress is increased, the axial strain increased with a high initial rate. This strain rate decreased as a power function of time. After 7–20 h, it stabilized at a seemingly constant value. These two distinct creep phases existed at all stress levels except the final one for all the tests. We treated the former phase as the transient creep and the latter phase as steady-state creep. The “steady-state” is true only for short durations. It does not remain constant with time. This will be shown later. Since most stress levels were maintained for no less than 3 days or 72 h, the steady-state creep lasted no less than 50 h, but mostly not more than 60–70 h (transient creep took 7–20 h). Shortly prior to failure, each specimen experienced an accelerating deformation. We treated this phase as accelerating creep. In a special case, if a specimen failed right after a loading increase, the accelerating creep may develop into failure extremely rapidly. In the following analysis, emphases will be given to tests 01023363-1-CU, 01023364-1-CU and 01023665-2-CU, because these tests experienced more stress steps and suffered less temperature influence.

### 2.1. Transient creep

Power and exponential functions have been checked by curve fitting to the transient creep data. The power function in Eq. (1) gives a significantly better fit. This agrees with Cruden [14].

$$\varepsilon_{tr} = \varepsilon_0 + \alpha t^\beta, \quad (1)$$

where  $\varepsilon_0$  is the initial axial strain,  $\alpha$  and  $\beta$  are material constants. Fig. 3 gives the axial strain–time plots and fitting curves for tests 01023363-1-CU, 01023364-1-CU and 01023665-2-CU. Fig. 3 is constructed in such a way in which all the axial strain–time plots are adjusted to zero intercepts. The equations for the curves were estimated using nonlinear regressions in the Excel SOLVER of Microsoft Office 2000 (Microsoft, Redmond, WA). The constants  $\alpha$  and  $\beta$  in each equation were estimated by maximizing the Pseudo- $R^2$ , the ratio of the regression sum of squares to the total sum of squares. This ratio explains the proportion of variance accounted for in the dependent variable by the model. It

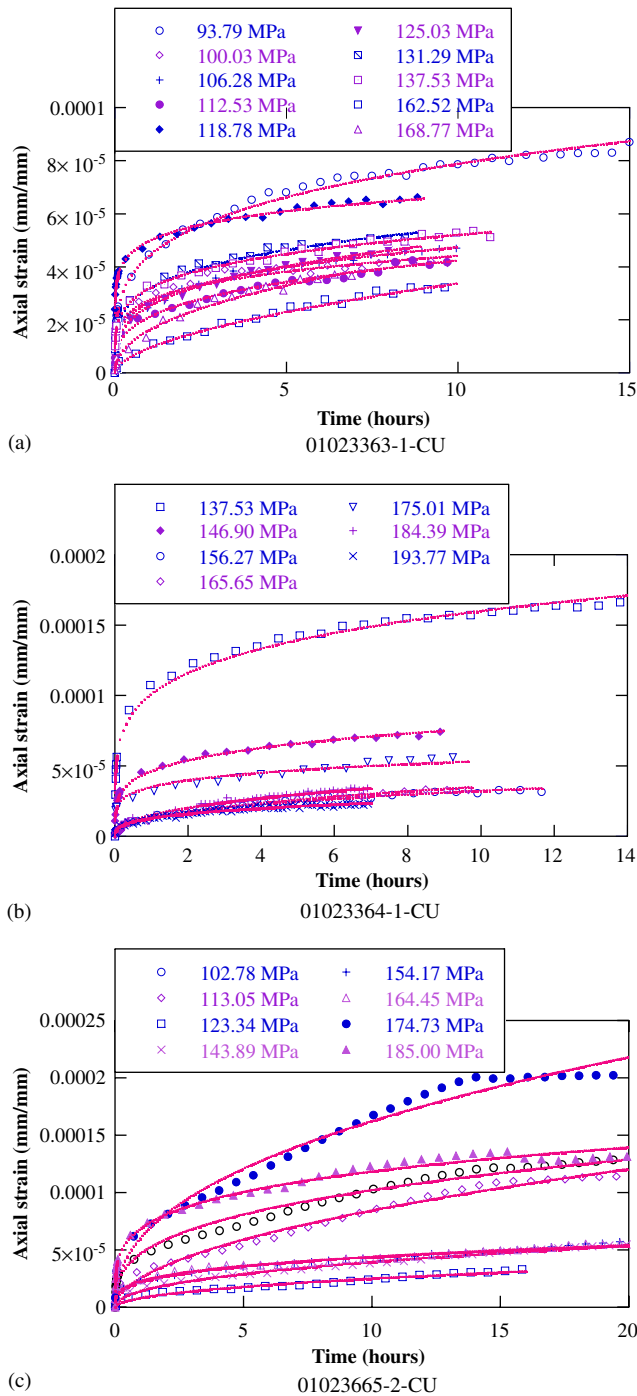


Fig. 3. Experimental axial strain–time plots for transient creep and fitting curves at stress levels given in inserts.

is equivalent to the  $R^2$ , the coefficient of determination, in linear regression. The values of  $\alpha$ ,  $\beta$  and Pseudo- $R^2$  in all the equations are listed in Table 3.

All the Pseudo- $R^2$ s are high, which indicates that all the curves fit the experimental plots well. As a general trend,  $\beta$  increases with stress. By taking the derivative of Eq. (1) with respect to time  $t$ , the strain rate for the

Table 3  
Values of  $\alpha$ ,  $\beta$  and Pseudo- $R^2$  for the estimated equations for the fitting curves in Fig. 3

Stress (MPa)	$\alpha$	$\beta$	Pseudo- $R^2$
01023363-1-CU			
93.79	4.4E-05	0.251	0.99
100.03	2.7E-05	0.207	0.98
106.28	2.7E-05	0.250	1.00
112.53	2.1E-05	0.301	0.99
118.78	5.0E-05	0.126	1.00
125.03	2.5E-05	0.291	1.00
131.29	3.2E-05	0.233	0.99
137.53	3.2E-05	0.213	1.00
162.52	9.5E-06	0.553	0.99
168.77	1.6E-05	0.441	0.99
01023364-1-CU			
137.53	1.0E-04	0.199	0.99
146.90	4.7E-05	0.217	0.99
156.27	1.4E-05	0.374	0.99
165.65	1.3E-05	0.439	0.99
175.01	3.5E-05	0.180	0.96
184.39	1.5E-05	0.411	0.99
193.77	1.3E-05	0.304	0.97
01023665-2-CU			
102.78	4.7E-05	0.335	0.98
113.05	2.6E-05	0.512	0.98
123.34	8.5E-06	0.475	0.97
143.89	1.4E-05	0.445	0.99
154.17	2.2E-05	0.303	0.98
164.45	2.3E-05	0.278	0.98
174.73	6.1E-05	0.425	0.98
185.00	6.9E-05	0.235	0.99

transient creep is obtained as

$$\dot{\epsilon}_{tr} = \alpha \times \beta \times t^{\beta-1}. \quad (2)$$

Eq. (2) takes the same form as the empirical law for rock salt proposed by Andrade (1910), quoted by Jaeger and Cook [25], and proposed by Dusseault [26] for transient creep. In Andrade’s study the exponent of  $t$  was  $-2/3$ . Our exponents of  $t$  are calculated based on the values of  $\beta$  in Table 3. We obtained the mean  $-0.68$  with a standard deviation 0.11.

### 2.2. Transition from transient creep to steady-state creep

The strain rate in transient creep can be calculated using Eq. (2). Fig. 4 shows the plot of the strain rate or transient creep rate as a function of time for test 01023364-1-CU at the 146.9 MPa stress level. The ratio of stress to axial strain versus time for the same test and the same stress level is plotted in the same coordinate system. As time goes by, both transient creep rate and stress/strain ratio decrease at fairly similar rate and in the same direction. This example plot indicates that a stabilized stress/strain ratio marks the end of the transient creep and the beginning of steady-state creep.

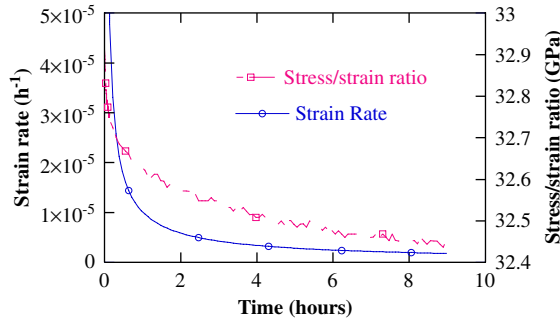


Fig. 4. Transient creep rate–time and stress/strain ratio–time curves for transient creep (test: 01023664-1-CU, stress level = 146.9 MPa).

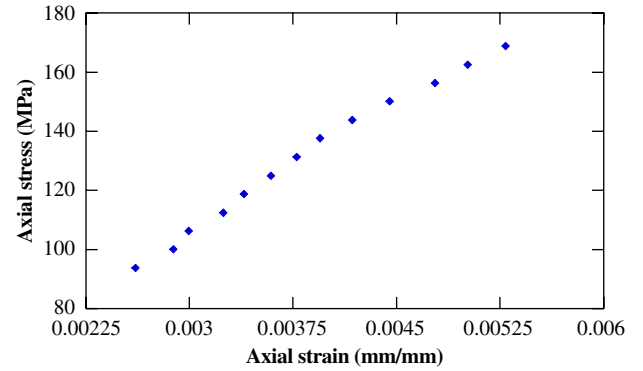
The stabilized stress/strain ratio defines the secant elastic modulus of the tuff [25]. The transient creep is essentially caused by the elastic aftereffect of the specimen. The elastic aftereffect is due to the thermo-elastic property of the specimen. A detailed discussion of this can be found in Timoshenko [27].

Picking the axial stress and axial strain at the end of transient creep for each stress level, and plotting these pairs of values in a stress–strain coordinate system for each test, Fig. 5 is obtained. The lower portions of the stress–strain plot for tests 01023363-1-CU and 01023665-2-CU and the entire plot for test 01023664-1-CU approximately lie on straight lines. This phenomenon reveals the following fact: within the straight range, axial stress and axial strain are approximately directly proportional. When the stresses exceed 143.79 MPa for test 01023363-1-CU and 174.73 MPa for test 01023665-2-CU, the plots of stress versus strain, where the transition from transient to steady-state creep occurs, started to deviate from their straight trends. This indicates that the elastic limit has been exceeded. Beyond the elastic limit, the specimen was softening, the transient creep ends with a higher strain rate, and a unit stress increment results in a larger strain response. For test 01023364-1-CU, the entire stress–strain plot is approximately linear, which means that the elastic limit had not been exceeded before the specimen failed.

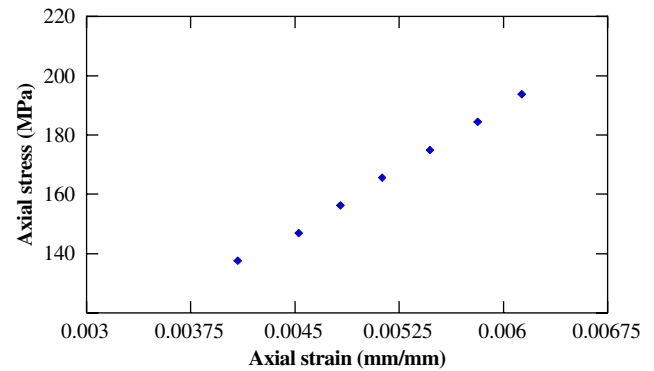
Costin and Holcomb [24] suggested that rock loaded in compression initially responds elastically. When the applied stresses reach a sufficient magnitude, the stress intensity factor associated with the most favorably oriented cracks reaches the critical value and these cracks begin to grow.

### 2.3. Steady-state creep

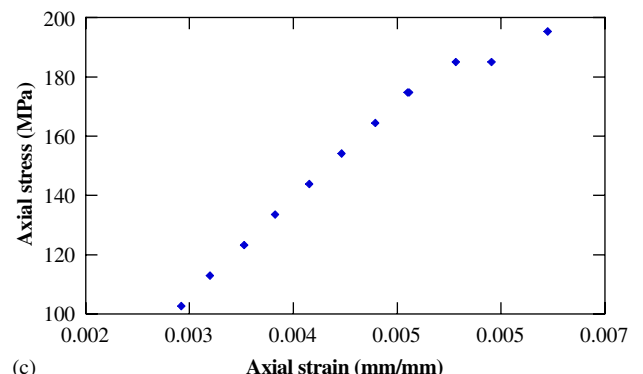
The temperature-induced strain was not seriously influential in transient creeps because the transient creep rates were relatively high. Comparatively strain rates in steady-state creep, or steady-state creep rates, were so small that they were extremely easily influenced by



(a) 01023363-1-CU



(b) 0102364-1-CU



(c) 01023665-2-CU

Fig. 5. Plots of stress and strain magnitudes at which the transition takes place from transient to steady-state creep for three tests at multi levels of constant stress.

temperature-induced strain. The Appendix gives the procedure of how the temperature-induced strain is removed from the strain measurement, i.e. how the net steady-state creep rate is estimated. The multivariate linear regression method is used to estimate average steady-state creep rate for a certain time span. Because most of the steady-state creeps were maintained for 50–70 h, we chose the lower limit bound, i.e. 50 h as a consistent systematic constant time unit to estimate the steady-state creep rate, with which we examined how the steady-state creep rates changed with stress. At some stress levels, the steady-state creeps lasted for 100–200 h.

For those cases, two, three or four time units (50 h) may be extracted. We used those long-lasting steady-state creep data to explore whether or not the steady-state creep rates changed with time in the long run and how they changed. Table 4 lists steady-state creep rates for the first time unit (0–50 h) interval for all the tests. Fig. 6 shows plots of steady-state creep rate versus stress for

tests 01023363-1-CU, 01023364-1-CU, 01023665-2-CU and 01023582-3-CU over the first 50 h.

In the first 50 h, steady-state creep rates are generally in the order of  $10^{-7} \text{ h}^{-1}$  (Table 4). The plots of steady-state creep rate versus stress for the four tests follow the same or similar form of nonlinear functions. As stress increases, this relation becomes clearer. A power function is the best fit for test 01023363-1-CU that experienced more stress levels than the others. The same form of power functions may also be the best description for steady-state creep rate–stress relationships for the other three tests. Scholz [22] stated that creep rate can often be given as a power function of stress, with the exponent near unity for very small stresses and greater than unity for moderate stresses.

All the tests experienced one or two stress levels in which the steady-state creeps were maintained for 100–200 h. These results of long-lasting steady-state creep allowed us to examine whether or not the so-called steady-state creep rate changed over longer test duration. We divided the duration for each stress level by 50 h (one time unit) so that two to four 50-h time units were obtained. Strain rates were estimated for each time unit and are listed in Table 5. Table 5 suggests that in the long duration the strain rate in the steady-state creep is not constant. From 0–50 h to 50–100 h, five go down and three go up. There are three stress levels that contain three or four time units. Axial strain versus time was determined for each time unit for these stress levels. The axial strain was estimated in the way in which the temperature-induced strain was removed from the strain

Table 4  
Steady-state creep rate for the first 50 hours for all the tests

Stress (MPa)	Strain rate ( $\text{h}^{-1}$ )	Stress (MPa)	Strain rate ( $\text{h}^{-1}$ )
<i>01023363-1-CU</i>		<i>01023665-2-CU</i>	
93.79	3.53E-07	102.78	2.76E-07
100.03	2.60E-08	113.05	3.32E-07
106.28	2.31E-07	123.33	2.35E-07
118.78	2.55E-07	143.88	2.31E-07
125.03	2.32E-07	154.18	2.76E-07
131.28	3.56E-07	164.43	6.18E-07
137.53	3.06E-07	174.73	6.30E-07
143.79	3.72E-07	174.73	5.05E-07
150.03	5.49E-07	185.01	5.15E-07
156.27	6.99E-07	<i>01023582-3-CU</i>	
162.52	6.30E-07	166.53	2.29E-07
<i>01023364-1-CU</i>		173.38	1.41E-07
137.53	4.62E-07	180.23	2.58E-07
146.90	3.78E-07	187.09	2.34E-07
165.65	4.29E-07	193.94	3.57E-07
175.01	6.57E-07	200.79	3.91E-07
184.39	6.17E-07	<i>01015465-CU</i>	
193.77	3.52E-07	102.75	1.35E-07
		123.35	4.58E-07

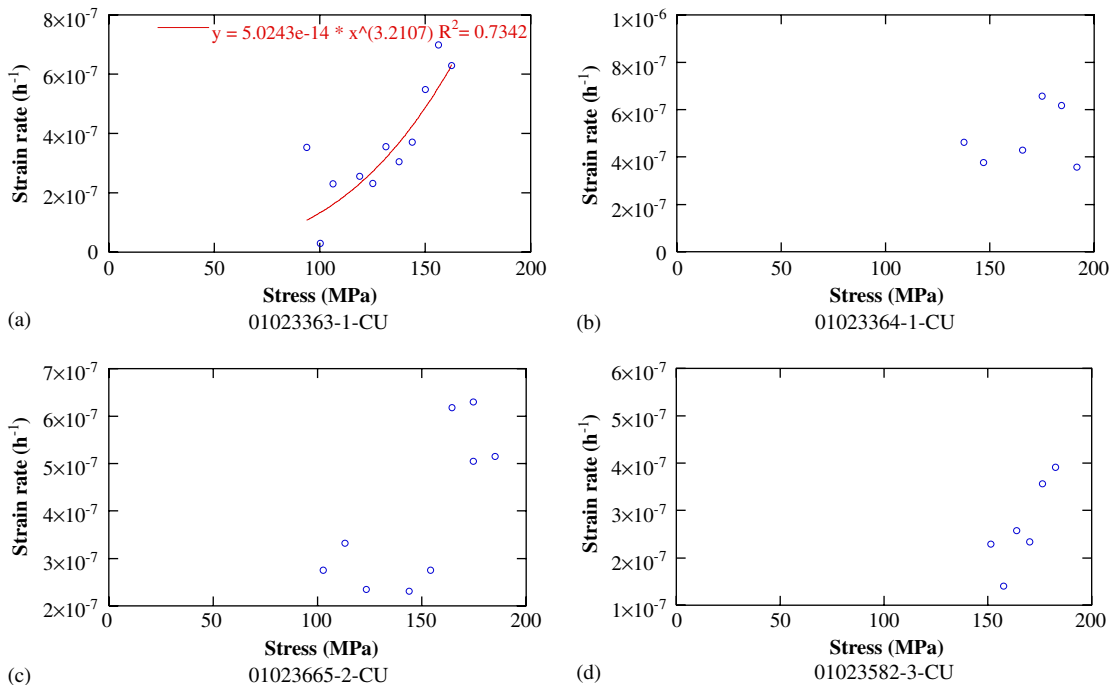


Fig. 6. Steady-state creep rate increases nonlinearly as a function of stress.

Table 5  
Steady-state creep rate dependent on time

Stress (MPa)	Strain rate ( $\text{h}^{-1}$ )		
	50–100 h	100–150 h	150–200 h
01023363-1-CU 118.78 143.78	9.27E-08 4.89E-07		
01023364-1-CU 137.53	1.73E-07		
01023665-2-CU 164.45 174.73	2.93E-07 2.00E-07	7.94E-08	6.45E-08
01023582-3-CU 173.38	6.59E-08	-1.93E-07	
01015465-CU 102.79 123.35	3.52E-07 4.71E-07	2.59E-07	

measurement. The temperature was adjusted to 28 °C, the average temperature for the tests. Fig. 7 gives the plots of measured axial strain–time, estimated axial strain–time and measured temperature–time for each stress level.

The slopes of the first two strain–time broken lines in Fig. 7 decrease with time. The third one goes up and then down. As a general trend, all three broken lines decrease in slope with time, which means as time goes by the so-called steady-state creep rate actually decreases. Table 5 and Fig. 7 suggest that the tuff does not have real steady-state creep when it is loaded beyond a certain duration. Costin [18] proposed that if a material is stressed below a threshold stress level and allowed to creep, the creep rate should decay to zero over time and no failure will occur. If the threshold stress level is exceeded, the damage level will continue to evolve, resulting in an eventual acceleration of the creep rate and failure. Dusseault [26] stated that low porosity silicates cannot display significant steady-state creep under engineering conditions. Ladanyi [19] believed that the dominating mechanisms for the creep test and rapid fracture test are different in the method of overcoming the energy barrier. In the fracture test, the energy is supplied by the continuously increasing stress, which drives the cracks to extend and interact. In creep tests, at a constant stress, cracks propagate into a stable position and stop. Further growth occurs when the energy barrier is lowered by a stress corrosion reaction at the crack tip. We conducted 65 uniaxial compression tests on the same type of tuff, and observed two threshold stresses by exploring stress–strain curves: the first one is about 50% of ultimate strength, and the second one is about 90% of ultimate strength. The first threshold stress marks the start of microfracturing and the second

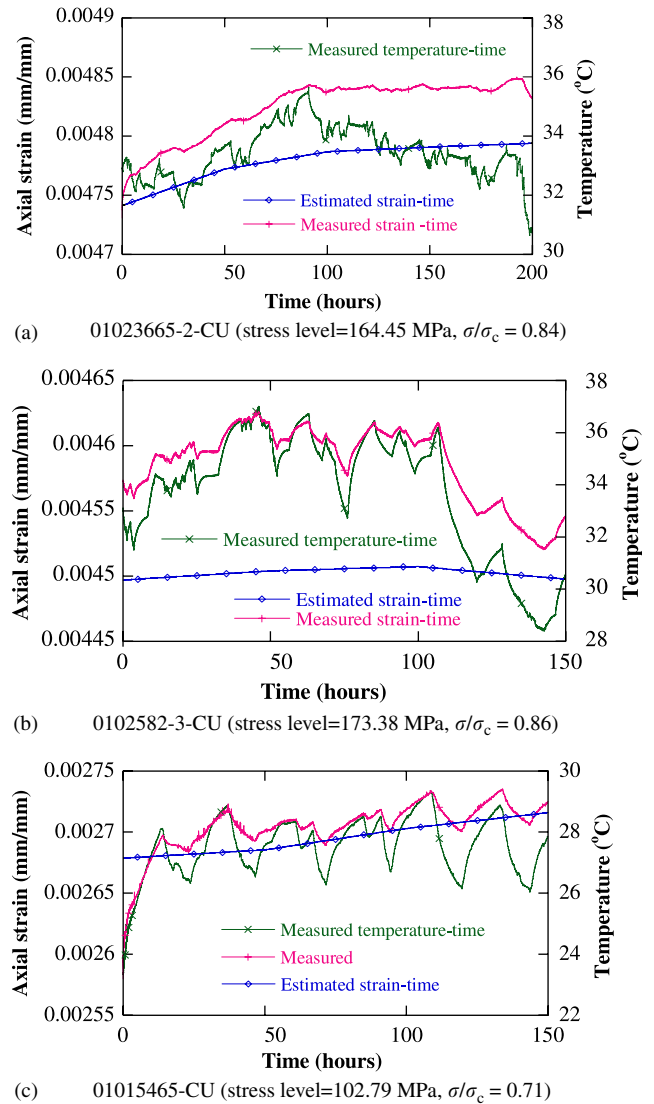


Fig. 7. Estimated strain, measured strain and measured temperature versus time in steady-state creep (unit of strain rate:  $\text{h}^{-1}$ ;  $\sigma_c$  = ultimate strength).

one marks the onset of specimen failure [28]. The average short-term strength of the same type tuff is 219.3 MPa, which was determined according to ASTM D 2938 [29] by Ma [28]. The steady-state creep rates shown in Fig. 7 were obtained at 164.45 MPa for test 01023665-2-CU, 173.38 MPa for test 0102582-3-CU and 102.79 MPa for test 01015465-CU. These stress levels have obviously exceeded 50% of the average short-term strength for the same type tuff.

2.4. Accelerating creep

Accelerating creep occurred at the final stress level for each test and led to failure of the specimen. If a specimen failed right after a loading increase, this stage could not be observed. Only one of the five tests exhibited accelerating creep (Fig. 8). Accelerating creep

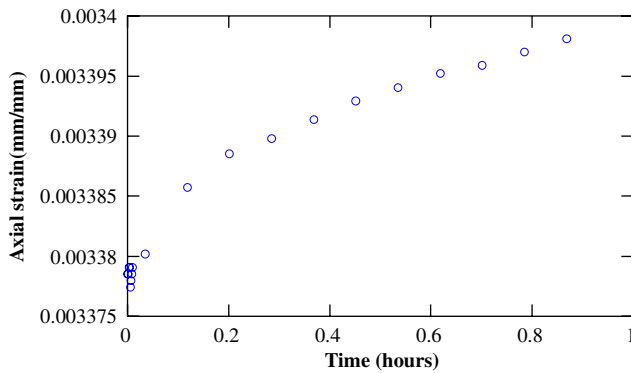


Fig. 8. Accelerating creep (test: 01015465-CU).

progressed quickly. At this phase the specimen had been damaged to such an extent that it could no longer resist the applied load. Once a rock entered this stage it inevitably failed unless it was unloaded. Between steady-state creep and accelerating creep there must be another critical transition point. The second threshold stress that occurs at about 90% of ultimate strength determined by Ma [28] may be this critical transition point. Cruden [30] and Kranz and Scholz [16] believe that accelerating creep starts when a critical crack density is reached.

### 3. Discussion and conclusions

We can speculate that the strain at failure induced by creep corresponds to the strain the samples would reach if a “conventional” complete stress–strain test were performed, i.e. that the strain at failure (approximately?) equals the strain that would be reached at the same (post peak) stress. This would parallel the proposition by Haimson and Kim [31] that cyclic fatigue testing leads to failure at a stress–strain point defined by the post peak stress–strain curve. While this concept has been questioned, or at least proposed to be subject to a need for more evidence [32], it certainly has been reinforced by the evidence presented by Wawersik and Brace [33] and especially Haimson [34,35]. Martin and Chandler [36] present particularly strong evidence for the case that cyclic loading (admittedly starting from a no stress condition, rather than cycling of constant amplitude about a (large) fraction of the ultimate strength) leads to a post peak stress–strain curve quite similar to the one obtained from a monotonic beyond peak loading. De Proft et al. [37] give an example of tensile testing on limestone where the cyclic test (albeit with two cycles only) results in a post peak softening curve quite similar to the one obtained under monotonic displacement increase. Another argument in support of the proposition that sustained loading at an elevated but below peak stress level may lead to the post-peak curve is the observation by Hudson [38], Hudson et al. [39], and

Hudson and Brown [40] that repeated (“cyclic”) post-peak relaxation followed by reloading leads to a “unique” post-failure curve, i.e. the repeated stress–strain curves rejoin a curve very similar to the one obtained from monotonic straining. Similar observations are reported by Peng [41]. The argument may be somewhat complicated by the fact that the post-peak stress–strain curve is a function of the strain rate at which it is obtained [42]. Stavrogin and Tarasov [42] (Sections 3.3.1 and 3.3.3) present strong evidence that for most rock types (but not for the evaporites rock salt and sylvinitite) the post-peak drop consistently is steepest at the slowest strain rate for which it is measured. Presumably it would be this steepest (least energy consuming) curve to which specimens under creep would strain. Overall similar patterns of post-peak dependency on strain rate have been observed by Peng and Podnieks [43] (for five (non-evaporite) rock types), Peng [41], Kawamoto and Saito [44], and Houpert [45]. However, some deviation from this pattern has been observed by Peng and Podnieks [43], for a tuff, by Peng [41] for a marble and a granite, and by Houpert [45] for a marble.

Wawersik [46] presents strong evidence that creep failure, at sustained stresses below the peak stress, or “strength”, leads to failure strains corresponding quite closely to strains observed in quasi static determinations of the complete stress–strain curve. This includes observations for three very different rock types, two of which are Class II type [47].

We can only speculate, because we do not have a good definition of the post-peak stress–strain curve of the tested tuff. What we do know beyond any doubt is that the tested tuff is extremely brittle, highly likely of Class II type. (Even when tested in uniaxial compression under controlled strain rates, at extremely slow strain rates (down to  $10^{-8} \text{ s}^{-1}$ ), upon reaching the peak strength the specimens fail instantly and violently [28].)

The main results can be summarized as:

- (1) Transient creep rate for the welded Topopah Spring tuff can be well described by a power function of time. Transient creep is marked by the stabilized stress/strain ratio that defines the secant elastic modulus. Transient creep is caused by the elastic aftereffect.
- (2) For the welded Topopah Spring tuff, the so-called steady-state creep rate is very low. Below the elastic limit, it typically varies in the range of  $10^{-7} \text{ h}^{-1}$ . The so-called steady-state creep rate decreases with time. There is no real steady-state creep for the welded Topopah Spring tuff.
- (3) Within the first 50 h, the so-called steady-state creep rate may be described as a power function of stress.
- (4) Accelerating creep progressed quickly. It marks the onset of the specimen failure.

## Acknowledgments

This paper was prepared by University of Nevada Reno pursuant to a Cooperative Agreement fully funded by the United States Department of Energy, and neither University and Community College System of Nevada nor any of its contractors or subcontractors nor the United States Department of Energy, nor any person acting on behalf of either

Makes any warranty or representation, express or implied, with respect to the accuracy, completeness, or usefulness of the information contained in this report, or that the use of any information, apparatus, method, or process disclosed in this report may not infringe privately owned rights or

Assumes any liabilities with respect to the use of, or for damages resulting from the use of, any information, apparatus, method or process disclosed in this report. Reference herein to any specific commercial product, process, or service by trade name, trademark, manufacturer, or otherwise, does not necessarily constitute or imply its endorsement, recommendation, or favoring by the United States Department of Energy. The views and opinions of authors expressed herein do not necessarily state or reflect those of the United States Department of Energy.

We would like to thank Mr. Rick Blitz for assistance with testing, and Mr. Jamie Gonzalez, DOE Technical Task Representative for overall help with this investigation, and in particular the organization of sample acquisition.

## Appendix. Thermal correction

The temperature-induced strain is given in [48] as

$$\varepsilon_{\text{temp}} = (\alpha - \alpha_g + \beta/F) \times \Delta T, \quad (3)$$

where  $\alpha$  is the coefficient of thermal expansion of the specimen,  $\alpha_g$  the coefficient of thermal expansion of the gage material,  $\beta$  the temperature coefficient of electrical resistivity of the grid conductor,  $F$  the gage factor of the strain gage,  $\Delta T$  the temperature change from the arbitrary initial reference temperature.

In Eq. (3) all of the coefficients within the parenthesis are themselves functions of temperature. If we ignore their temperature dependency for a relative small change of temperature, then  $\varepsilon_{\text{temp}}$  is approximately linear with  $\Delta T$ . The justification for this assumption will be verified with regression result.

Let the steady-state creep rate be  $\dot{\varepsilon}$ , the stress-induced strain is given by

$$\varepsilon_{\text{stress}} = \dot{\varepsilon} \times t. \quad (4)$$

The strain measured in steady-state creep tests is the sum of temperature-induced strain and stress-induced

Table 6  
Results of estimation for coefficients of  $\Delta T$  and  $t$

Intercept	$\Delta T$	$t$	Adjusted $R^2$
0–50 h 0.004207	1.12E-05	1.41E-07	0.994
50–100 h 0.004234	1.04E-05	6.59E-08	0.954
100–150 h 0.004220	1.16E-05	−1.93E-07	0.996

strain

$$\varepsilon_{\text{ss}} = \varepsilon_{\text{temp}} + \varepsilon_{\text{time}} \quad (5)$$

or

$$\varepsilon_{\text{ss}} = (\alpha - \alpha_g + \beta/F) \times \Delta T + \dot{\varepsilon} \times t. \quad (6)$$

By regressing  $\varepsilon_{\text{ss}}$  on  $\Delta T$  and  $t$ , the algebraic sum within the parenthesis and  $\dot{\varepsilon}$  in Eq. (6) can be estimated. Let the 173.38 MPa stress level for test 0102582-3-CU be an example. Table 6 gives results of estimation for three time intervals, 50 h each. All three the time intervals have very high adjusted  $R^2$ . Setting the initial reference temperature as 28 °C, the corrected strain–time line segments are shown in Fig. 7b. The measured strain–time data and measured temperature–time data are also plotted.

## References

- [1] OCRWM (Office of Civilian Radioactive Waste Management), Website: <http://www.ocrwm.doe.gov>, September 2004.
- [2] OCRWM. Geology of the ECRB cross drift-exploratory studies facility, Yucca Mountain Project, Yucca Mountain, NV. Denver, Colorado: Bureau of Reclamation and US Geological Survey; 1999.
- [3] ASTM D 4543-85 (Reapproved 1991), Standard practice for preparing rock core specimens and determining dimensional and shape tolerances. Annual book of ASTM standards, Section 4, construction, vol. 04.08, Soil and Rock, Building Stones, Conshohocken, PA: American Society for Testing and Materials.
- [4] Martin III. RJ, Price RH, Boyd PJ, Noel JS. The influence of strain rate and sample inhomogeneity on the moduli and strength of welded tuff. Int J Rock Mech Min Sci Geomech Abstr 1993;30:1507–10.
- [5] Rautman CA, Engstrom DA. Geology of the USW SD-12, Drill Hole Yucca Mountain, Nevada. Sandia report, SAND96-1368, UC-814, Sandia National Laboratories, 1996a.
- [6] Rautman CA, Engstrom DA. Geology of the USW SD-7, Drill Hole Yucca Mountain, Nevada. Sandia report, SAND96-1474, UC-814, Sandia National Laboratories, 1996b.
- [7] Engstrom DA, Rautman CA. Geology of the USW SD-9, Drill Hole Yucca Mountain, Nevada. Sandia report, SAND96-2030, UC-814, Sandia National Laboratories, 1996.
- [8] DOE/RW-0549, Yucca Mountain site suitability evaluation. DOE report, Website: [http://yucca-web2.ymp.gov/documents/sse\\_a](http://yucca-web2.ymp.gov/documents/sse_a), February 2002.

- [9] Shen B, Stephansson O, Einstein HH, Bidjan G. Coalescence of fractures under shear stresses in experiments. *J Geophys Res* 1995;100(B4):5975–90.
- [10] Wong RHC, Chau KT, Tang CA, Lin P. Analysis of crack coalescence in rock-like materials containing three flaws-part I: experimental approach. *Int J Rock Mech Min Sci* 2001;38:909–24.
- [11] Brace WF, Bombolakis EG. A note on brittle crack growth in compression. *J Geophys Res* 1963;68(12):3709–13.
- [12] Walsh JB. The effect of cracks on the uniaxial elastic compression of rocks. *J Geophys Res* 1965;70(2):399–411.
- [13] Brace WF, Paulding Jr. BW, Scholz CH. Dilatancy in the fracture of crystalline rocks. *J Geophys Res* 1966;71(16):3939–53.
- [14] Cruden DM. The form of the creep law for rock under uniaxial compression. *Int J Rock Mech Min Sci* 1971;8:105–26.
- [15] Lajtai EZ. A theoretical and experimental evaluation of the Griffith theory of brittle fracture. *Tectonophysics* 1971;11: 129–56.
- [16] Kranz RL, Scholz CH. Critical dilatant volume of rocks at the onset of tertiary creep. *J Geophys Res* 1977;82(30):4893–8.
- [17] Horii H, Nemat-Nasser S. Compression-induced microcrack growth in brittle solids: axial splitting and shear failure. *J Geophys Res* 1985;90(B4):3105–25.
- [18] Costin LS. Time-dependent damage and creep of brittle rock. In: *Damage mechanics and continuum modeling*, proceedings of 2 sessions sponsored by the Engineering Mechanics Division of the American Society of Civil Engineers in Conjunction with the ASCE Convention, Detroit, MI, 1985.
- [19] Ladanyi B. Time-dependent response of rock around tunnels. In: *Comprehensive rock engineering, principles, practice and projects*, vol. 3. Oxford: Pergamon Press; 1993. p. 77–112.
- [20] Lemaitre J. *A course on damage mechanics*. New York: Springer; 1992.
- [21] Martin RJ, Noel JS, Boyd PJ, Price RH. Creep properties of the paintbrush tuff recovered from Borehole USW NRG-7/7A: data Report. SAND95-1759, UC-814, Sandia National Laboratories, 1997.
- [22] Scholz CH. Experimental study of the fracturing process in brittle rock. *J Geophys Res* 1968;73(4):1447–54.
- [23] Scholz CH. Microfracturing and the inelastic deformation of rock in compression. *J Geophys Res* 1968;73(4):1417–32.
- [24] Costin LS, Holcomb DJ. A continuum model of inelasticity deformed brittle rock based on the mechanics of microcracks. In: *Constitutive laws for engineering materials theory and application*, proceedings of the international conference, Tucson, AZ, 1983.
- [25] Jaeger JC, Cook NGW. *Fundamentals of rock mechanics*. 3rd ed. London: Chapman & Hall; 1979. p.79 and 311.
- [26] Dusseault MB, Fordham CJ. Time-dependent behavior of rocks. In: *Comprehensive rock engineering, principles, practice and projects*, vol. 3. Oxford: Pergamon Press; 1993.
- [27] Timoshenko SP. *History of strength of materials: with a brief account of the history of theory of elasticity and theory of structures*. New York: McGraw-Hill; 1953. p. 336–357.
- [28] Ma L. Experimental investigation of time dependent behavior of welded Topopah Spring tuff, Dissertation, University of Nevada, Reno, 2004.
- [29] ASTM D 2938-95, Standard test method for unconfined compressive strength of intact rock core specimens. Annual book of ASTM standards, section 4, construction, vol. 04.08, soil and rock, building stones, Conshohocken, PA: American Society for Testing and Materials.
- [30] Cruden DM. The static fatigue of brittle rock under uniaxial compression. *Int J Rock Mech Min Sci Geomech Abstr* 1974;11:67–73.
- [31] Haimson BC, Kim CM. Mechanical behavior of rock under cyclic fatigue. In *stability of rock slopes*, proceedings of 13th symposium on rock mechanics, University of Illinois, Urbana, 1972. p. 845–63.
- [32] Farmer I. *Engineering behaviour of rocks*. 2nd ed. London: Chapman & Hall; 1983. p. 138.
- [33] Wawersik WR, Brace WF. Post-failure behavior of a granite and diabase. *Rock Mech* 1971;3:61–85.
- [34] Haimson BC. Mechanical behavior of rock under cyclic loading. In: *Advances in rock mechanics*, proceedings of the third congress of the international society for rock mechanics, vol. II. Denver, CO, National Academy of Sciences, Washington, DC, 1974. p. 373–78.
- [35] Haimson BC. Effect of cycling loading on rock. In: *Dynamic geotechnical testing*, ASTM STP 654. Philadelphia: American Society for Testing and Materials; 1978. p. 228–45.
- [36] Martin CD, Chandler NA. The progressive failure of lac du bonnet granite. *Int J Rock Mech Min Sci Geomech Abstr* 1994;31:643–59.
- [37] De Proft K, Sluys LJ, De Wilde WP. A combined experimental-numerical study to monotonic and cyclic behaviour of limestone. In: *Damage and fracture mechanics*, vol. VII. Southampton Boston: WIT Press; 2003. p. 257–64.
- [38] Hudson JA. Effect of time on the mechanical behaviour of failed rock. *Nature* 1971;232:185–6.
- [39] Hudson JA, Crouch SL, Fairhurst C. Soft, stiff and servo-controlled testing machines: a review with reference to rock failure. *Eng Geol* 1972;6:155–89.
- [40] Hudson JA, Brown ET. Studying time-dependent effects in failed rock. In: *New horizons in rock mechanics*, proceedings of 14th symposium on rock mechanics, Pennsylvania State University, 1973. p. 25–34.
- [41] Peng S. Time-dependent aspects of rock behavior as measured by a servo-controlled hydraulic testing machine. *Int J Rock Mech Min Sci Geomech Abstr* 1973;10:235–46.
- [42] Stavrogin AN, Tarasov BG. Experimental physics and rock mechanics. In: Fairhurst C, editor. *Lisse: A.A. Balkema Publishers*; 2001.
- [43] Peng S, Podnieks ER. Relaxation and the behavior of failed rock. *Int J Rock Mech Min Sci* 1972;9:699–712.
- [44] Kawamoto T, Saiko T. The behaviour of rock-like materials in some controlled strain rates. In: *Advances in rock mechanics*, proceedings of the third congress of the International Society for Rock Mechanics, vol. II, Denver, CO, National Academy of Sciences, Washington, DC, 1974. p. 161–66.
- [45] Houpert R. Le Rôle du Temps dans le Comportement à la Rupture des Roches. In: *Advances in rock mechanics*, proceedings of the third congress of the international society for rock mechanics, vol. II, Denver, CO, National Academy of Sciences, Washington, DC, 1974. p. 325–29.
- [46] Wawersik WR. Time-dependent rock behavior in uniaxial compression. In: *New horizons in rock mechanics*, proceedings of 14th symposium on rock mechanics, Pennsylvania State University, 1973. p. 85–106.
- [47] Wawersik WR, Fairhurst C. A study of brittle rock fracture in laboratory compression experiments. *Int J Rock Mech Min Sci* 1971;7:561–75.
- [48] Poore MW, Kesterson KF. Measuring the thermal expansion of solids with strain gages. *J Test Eval* 1978;6(2):89–102.